Robotica (2007) volume 25, pp. 549–565. © 2007 Cambridge University Press
doi:10.1017/S026357470700344X Printed in the United Kingdom

A uniform biped gait generator with offline optimization and online adjustable parameters

Lin Yang†*, Chee-Meng Chew†, Teresa Zielinska‡ and Aun-Neow Poo†

†*Control and Mechatronics Lab, Department of Mechanical Engineering, The National University of Singapore, 10 Kent Ridge Crescent, Singapore 119260, Singapore*
‡*Warsaw University of Technology, Institute for Aircraft Engineering and Applied Mechanics, 00-665 Warsaw, Poland*

(Received in Final Form: February 1, 2006. First published online: March 19, 2007)

SUMMARY
This paper presents the Genetic Algorithm Optimized Fourier Series Formulation (GAOFSF) method for stable gait generation in bipedal locomotion. It uses a Truncated Fourier Series (TFS) formulation with its coefficients determined and optimized by Genetic Algorithm. The GAOFSF method can generate human-like stable gaits for walking on flat terrains as well as on slopes in a uniform way. Through the adjustment of only a single or two parameters, the step length and stride-frequency can easily be adjusted online, and slopes of different gradients are accommodated. Dynamic simulations show the robustness of the GAOFSF, with stable gaits achieved even if the step length and stride frequency are adjusted by significant amounts. With its ease of adjustments to accommodate different gait requirements, the approach lends itself readily for control of walking on a rough terrain and in the presence of external perturbations.

KEYWORDS: Truncated Fourier Series; Genetic algorithm; Biped; Gait generation and adjustment.

1. Introduction

Walking robots' locomotion control architecture and algorithm design is on a roll.[1] Bipedal locomotion control, an important part of intensive research into humanoid robots in recent years, investigates the fundamentals of how a biped can achieve stable and adaptive walking on different terrains. The difficulty of bipedal robot locomotion control can be attributed to the nonlinearity of its dynamics, interaction with an unknown environment, and the existence of underactuation at the ankle joint during the stance phase.[2]

Many approaches have been proposed for the bipedal gaits generation. To reduce the complexity of the analysis, some researchers adopted a simplified dynamic model such as the inverted pendulum with certain assumptions on the robot's motion and structure.[3,4] Nakanishi *et al.* made use of recorded human gaits as the reference for robot trajectory planning.[5] Although human walking data are useful for gait analysis, there still exist significant differences between the dynamics of a bipedal robot and its human counterpart.[2]

*Corresponding author. Email: yanglin@nus.edu.sg

Some other researchers adopted a biologically inspired approach using the idea of the CPG (Central Pattern Generator).[6–11] In the CPG-based approach, bipedal trajectory generation has been achieved with the use of a network of neural oscillators.[12] Each neural oscillator can be implemented using a set of nonlinear coupled equations.[13] It has the desirable property of adaptation to the environment through entrainment. However, it is difficult not only to design the interconnection and feedback pathways of the neural oscillators, but also to manually tune the required parameters in order to achieve the desired walking characteristics. The advantage of the CPG-based approach is the possibility for real-time motion generation with a general method.

A popular approach used for joint trajectory planning for bipedal locomotion is based on the ZMP (zero moment point) stability indicator.[14–16] In many ZMP-based trajectory planning approaches, motion planning is presupposed and performed in the Cartesian space.[17–19] These motions typically have "bent-knee" postures in order to avoid the singularity problem when solving the inverse kinematics. The bent-knee posture has the disadvantage that it tends to require more effort from the joints and the resulting motion is not as natural as the human gait.[5] On the other hand, previous ZMP-based works give some motion assumptions but do not give much freedom for online motion adjustments, for example, one joint or body part is predetermined,[20] or trunk or waist compensatory motions are used to reduce the error between the desired ZMP and actual ZMP trajectory.[21]

The motivation for this research is to combine the ZMP stability indicator with the CPG concept to develop a ZMP-based CPG model, which can clarify the relationship between mathematical model and robot dynamics. Furthermore, it is aimed to give a uniform motion generation method with adjustable parameters for the universal locomotion stability. With this approach, stable bipedal walking gaits can be generated which also allows adjustments of the step length during walking, the walking rhythm, and adaptation to the environment. Referring to the knowledge gained from human gaits research on the function of the CPG in rhythm generation, it can be summarized that walking is just a basic function stored in our biological neural networks. During walking on different terrains, this function is modified

automatically according to human sense about the nature of the terrain.

In this paper, a Genetic Algorithm Optimized Fourier Series Formulation (GAOFSF) method is presented for generating joint trajectories for stable bipedal locomotion. In this approach, each joint angle trajectory is first modeled using a special Truncated Fourier Series (TFS). A set of constraints and objective functions is then identified and recurrently computed by Genetic Algorithm (GA)[22] to search for an optimal set of parameters for the TFS for a given biped. The resulting joint trajectories are then used to achieve both flat and sloped terrain locomotion with online adjustments of certain parameters to adapt to the nature of the terrain.

The algorithm is very general, which combines the knowledge of ZMP and CPG, and can be applied for motion generations besides the typical human-pattern walking. In addition, there is always space for adding trunk or waist compensatory motions to further improve the stability or generalize the approach to a 3D space. One of the advantages of GAOFSF is that trajectory generation is done directly in the joint space. As such, inverse kinematics computation is not required thus avoiding the singularity problem. The walking rhythm, step length, and walking pattern can also be adjusted online through tuning either a single or two parameters. Those parameters chosen as adjustable in GAOFSF have clear physical meanings for its walking patterns. Therefore, it brings the straightforward relationships between mathematic model and robotic dynamics. Furthermore, by using this designed TFS function here, fewer mathematic constraints are required than in other function approximations in the gaits generation, which will be discussed in Section 2.

The conceptual scheme of bipedal locomotion control using GAOFSF is shown in Fig. 1.

The offline part, consisting of block 1, 2, 3, 4, is responsible for the generation of walking pattern, and then giving adjustable walking pattern parameters to get the TFS pattern generator. Then, the online loop uses the elaborated generator to adjust walking motions automatically.

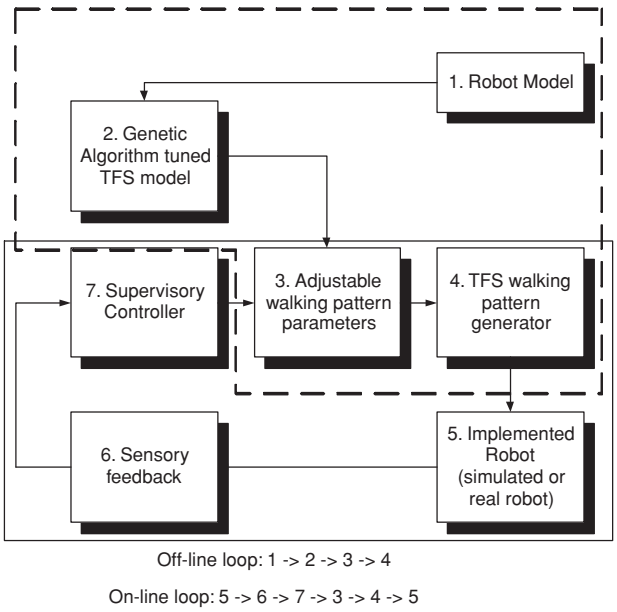

Fig. 1. Bipedal locomotion control scheme.

In this paper, we present the GAOFSF and its uses for motion adjustments. Some supervisory controllers will be discussed in the following reports. Section 2 describes the TFS, which generates the hip and knee joint angle trajectories. In Section 3, details of the objective functions, constraints, and the optimization process using GA are discussed. The resulting motions when the method is applied on a seven-link planar biped for flat-terrain walking, and for uphill and downhill terrains are presented in Section 4. Section 5, 6, and 7 discuss the joint position control and evaluate the results obtained from the dynamic simulation using Yobotics!, which demonstrates the validity of the proposed algorithm.

2. Truncated Fourier Series (TFS) Formulation

In the GAOFSF approach, a TFS formulation is used for the synthesis of hip and knee joint angle trajectories. It differs from the former work[23] representing joint trajectories of human walking by Fourier series function at the usage of parameters in Fourier series for real-time motion adjustments. Furthermore, it provides a way that the cosine part of Fourier series might not be necessary and thus can be tailored. In the presented approach, GA is used to search for the optimal values of the parameters in these formulations so as to achieve stable walking behavior with desirable characteristics for a given biped.

The bipedal robot used to illustrate the application of the proposed approach is a seven-link planar robot, as shown in Fig. 2. Its geometrical and inertial properties are given in Table I. It is made up of a trunk and two legs, with each leg comprising a thigh, a shank, and a foot. Each leg has three degrees of freedom, i.e., the hip–pitch joint H, the knee–pitch joint K, and the ankle-pitch joint A. T is the mid-point between the left and the right hip joints.

Gait synthesis for this bipedal robot involves first determining the hip–pitch and knee–pitch angle trajectories for each of the legs. The ankle-pitch angle trajectory of the swing leg is then determined based on the condition that it is always compliant with the ground surface. The ankle-pitch

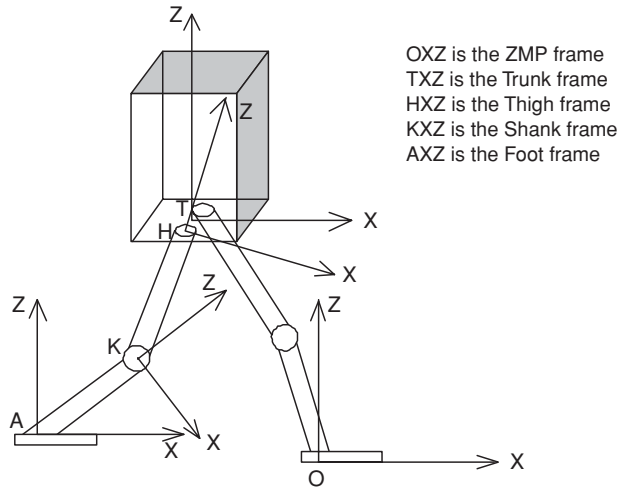

Fig. 2. Seven-link bipedal robot and coordinate systems.

https://doi.org/10.1017/S026357470700344X Published online by Cambridge University Press

Table I. Geometrical and inertial properties of the biped.

Link	Mass distribution	Mass (kg)	Moment of Inertia (kg·m^2) about y-axis	Size (m) ($L \times W \times H$) or ($L \times d$)
Trunk	Uniform	12	0.97	$0.2 \times 0.2 \times 0.45$
Thigh	Uniform	6	0.0456	0.3×0.02
Shank	Uniform	5	0.038	0.3×0.02
Foot	Uniform	1	0.03012	$0.3 \times 0.1 \times 0.02$

angle of the stance leg is used to maintain the body-pitch angle, which is set to be zero in this work.

The coordinate frames attached to the trunk (*TXZ*), the right thigh (*HXZ*), the right shank (*KXZ*), and the right foot (*AXZ*) are defined as shown in Fig. 2. An additional coordinate frame (*OXZ*) attached to the ankle joint of the stance foot is used as the reference frame for the zero-moment-point (ZMP). Referring to Fig. 2, define for the right leg,

Right Hip Angle, θ_{rh} = the angle of axis *HZ* from axis *TZ* in clockwise direction.

Right Knee Angle, θ_{rk} = the angle of axis *KZ* from axis *HZ* in clockwise direction.

The corresponding angles for the left leg, θ_{lh} and θ_{lk}, are similarly defined.

2.1. *Basic features of human gait*

In the literature, materials illustrating typical shapes of trajectories for hip and knee angles in one cycle of locomotion is easy to get,[24] but for a deeper insight into human motion properties we recorded and processed human gait using 3D VICON motion registration system and POLIYGON human motion analysis software. Fig. 3a gives the hip and knee trajectories for a 1.83 m tall person (74 kg weight). The reference frames are the same as defined for the biped model aforementioned. The gait analysis software verified the obtained data comparing it with the stored norms. From the gaits recorded by VICON, considering the fact that human body is physically different from a robot's rigid links, we elaborated Fig. 3b, which has captured the main features of Fig. 3a but gives a general form to make it applicable to robots. The trajectories for both legs are identical in shape but are shifted in time relative to each other by half of the walking period. For example, θ_{lh} for the left hip is identical to θ_{rh} for the right hip, except that θ_{lh} is time shifted by $(t_6 - t_0)/2$ w.r.t. θ_{rh}. The gait period is given by $2\pi/\omega_h$ where ω_h is defined as the gait frequency in radians per second (rad/s). It can also be noted that the joint angle trajectories can be separately looked by "offsets." The values of the defined offsets actually influence the biped's posture during walking. c_h denotes the hip angle offset. This is the value of both hip joint angles at the point they become equal, or at which the two thighs cross each other. c_k denotes the knee angle offset. This is the value of the knee angle when the knee is locked during part of the support phase. t_1 and t_2 denote the start and end time, respectively, of the lock phase. To give a freedom of the lock phase (from t_1 to t_2), which is not obviously shown in the human gait, is required because the physical pattern of the stance leg is tending to lift up the body and then be straightened. However due to the physical body constraints, it could be bent or overstretched a little referring to Fig. 3a, from $t = 0.14$ to 0.4 s, but the peak value is small; thus, it can be simplified in the robot whose links are all rigid as a lock phase. Nevertheless, Fig. 3b is still considered general because it will exactly resemble the human walking features if t_1 and t_2 in the TFS model optimization turn out to be coincided. Then there will be no lock phase, but it may ask a higher order TFS to give a curve with two different peaks, alternatively, another set of TFS for the period from t_1 to t_2 can be added into the computation.

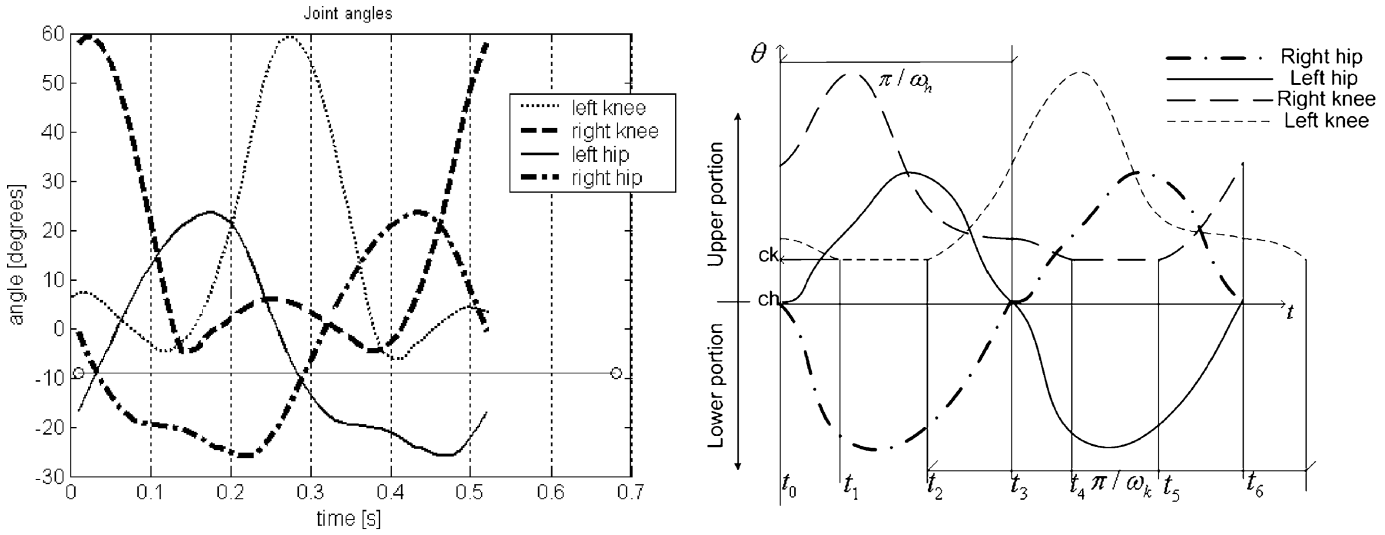

Fig. 3. (a) Human gaits on flat-terrain recorded by VICON. (b) Uniform gaits elaborated from human gaits features. *Right support:* $[t_2, t_5]$; *right swing:* $[t_0, t_2]$ and $[t_5, t_6]$; *left support:* $[t_0, t_2]$ and $[t_5, t_6]$; *left swing:* $[t_2, t_5]$.

https://doi.org/10.1017/S026357470700344X Published online by Cambridge University Press

Consider first the hip angle trajectories. They can be divided into an upper portion, θ_h^+, for which $\theta_h \geq c_h$, and a lower portion, θ_h^-, for which $\theta_h < c_h$. Thus, referring to Fig. 3b, for the two portions of the walking cycle, the hip joint angles for the two legs are given by

$$\begin{array}{llll} t \in [t_0,\ t_3] & \theta_{rh} = \theta_h^-(t) & & \theta_{lh} = \theta_h^+(t) \\ t \in [t_3,\ t_6] & \theta_{rh} = \theta_h^+(t - t_3) & & \theta_{lh} = \theta_h^-(t - t_3) \end{array} \tag{1}$$

here θ_{rh} and θ_{lh} are the right and the left hip joint angles, respectively.

Similarly, the right knee joint angle trajectory for different portions of the walking cycle is given by

$$\begin{array}{ll} t \in [t_0,\ t_4] & \theta_{rk} = \theta_{k1}(t + t_6 - t_5) \\ t \in [t_4,\ t_5] & \theta_{rk} = \theta_{k2} \\ t \in [t_5,\ t_6] & \theta_{rk} = \theta_{k1}(t - t_5) \end{array} \tag{2.1}$$

where θ_{k1} is the knee joint trajectory from the beginning of swing phase, denoted by t_5 for the right knee in Fig. 3b, to the instant in the support phase when the knee joint is locked, denoted by t_4 in Fig. 3b. θ_{k2} is the locked knee joint angle.

Similarly, referring to Fig. 3b, the joint angle for the left knee is given by

$$\begin{array}{ll} t \in [t_0,\ t_1] & \theta_{lk} = \theta_{k1}(t + t_6 - t_2) \\ t \in [t_1,\ t_2] & \theta_{lk} = \theta_{k2} \\ t \in [t_2,\ t_6] & \theta_{lk} = \theta_{k1}(t - t_2) \end{array} \tag{2.2}$$

where t_1 is the instant when the stance knee is locked and t_2 is the instant when the walking phases of the two legs are switched.

2.2. *Joint trajectory representation using TFS*

The Fourier Series of a periodic function of time $f(t)$ can be written as

$$f(t) = \frac{1}{2}a_0 + \sum_{i=1}^{\infty} a_i \sin\left(\frac{2\pi i}{T}t\right) + \sum_{i=1}^{\infty} b_i \cos\left(\frac{2\pi i}{T}t\right) \tag{3}$$

where a_i and b_i are constant coefficients and T is the period. The fundamental frequency is given by $\omega_1 = 2\pi/T$.

As discussed in the previous section, all the joint trajectories during a gait cycle can be divided into two portions. Each portion can be viewed as an odd function output according to the intersection with the angle axis. Therefore the sine series in the Fourier series function is simplified; a TFS is used to model each portion as follows

$$f(t) = \sum_{i=1}^{n} a_i \sin i\omega t + c_f \tag{4}$$

where a_i and c_f are constants to be determined and ω is the fundamental frequency determined by the desired period of the gait. The parameter n, which determines the number of terms in the Fourier series, is chosen as a trade-off between the accuracy of the approximation required and the computational load. The formulation as shown in Eq. (4) is used for the joint angles $\theta_h^+(t)$, $\theta_h^-(t)$, and $\theta_{k1}(t)$ as given in Eqs. (1) and (2). Although the function is periodic, only the first half of the period is needed for the joint angles. It is noted here that since the shapes of the upper and the lower portions are not symmetrical about the $(0, c_h)$ point, even if the full Fourier series is used, this cannot automatically give an equal time period for the upper and the lower portions of a walking motion. The use of the full Fourier series, as with other approximation functions, will therefore also require an additional mathematical constraint to fix the profile so that the upper and the lower portions intersect at the points $(0, c_h)$ and (T_s, c_h), T_s being the step period. As can be seen from the foregoing, the use of TFS allows for a reduced series with fewer parameters for the same approximation accuracy, and with fewer constraints required. This significantly reduces the subsequent computational load in the search for feasible and optimal solutions using GA.

Using Eqs. (1–4), and by inspection of the curves in Fig. 3b, the TFS for the hip–pitch angles are formulated as

$$\theta_{rh}, \theta_{lh} = \begin{cases} \theta_h^+ = \sum_{i=1}^{n} R \cdot A_i \sin i\omega_h(t - t_h^+) + c_h, & \text{where } \omega_h = \pi/(t_3 - t_0) = \pi/(t_6 - t_3) \\ \theta_h^- = \sum_{i=1}^{n} R \cdot B_i \sin i\omega_h(t - t_h^-) + c_h \end{cases} \tag{5}$$

where A_i and B_i are constant coefficients, θ_h^+ and θ_h^- are the upper and the lower portions, respectively, of the hip joint angle trajectory, and t_h^+ and t_h^- are time-shift values according to Eq. (1). R is an amplitude scaling parameter used for changing the step length. Initially, R is set to 1.

Similarly, the trajectories for the knee joint angles are expressed as

$$c\theta_{rk}, \theta_{lk} = \begin{cases} \theta_{k1} = \sum_{i=1}^{n} R \cdot C_i \sin i\omega_k(t - t_k) + c_k, & \text{where } \omega_k = \pi/((t_6 - t_2) + (t_1 - t_0)) \\ \theta_{k2} = c_k \geq 0 \end{cases} \tag{6}$$

where C_i are constant coefficients and t_k is the time shift.

Compared with other approximation approaches,[18,25–28] the advantages of using the TFS to synthesize the walking gait for bipedal robots are as follows:

1. With only a few terms in the series, it can represent quite accurately the shapes of the required joint trajectories for human-walking-inspired biped robot gait, for which

https://doi.org/10.1017/S026357470700344X Published online by Cambridge University Press

the upper and the lower portions are not symmetrical but individually are similar to half a sinusoid.
2. Each TFS used here is a simple expression that makes no mathematical assumption when considered as half of an odd function. The gait period is included directly. Other functions such as the Spline, Gaussian, or the full Fourier series function will add additional constraints to regulate the motion period as mentioned above.
3. Key parameters of the TFS can be easily adjusted online during walking to change the walking gait, either to change the desired pace or in response to external perturbations.

3. Gait Generation Algorithm Implementation Factors

In this section, the necessary algorithm implementation tools are discussed. The ZMP is used to ensure that the generated gait is feasible and stable, and the GA is used to search for the desired feasible and optimal gaits according to specified objective functions and within specified constraints.

3.1. Dynamic stability criterion—ZMP

The ZMP stability indicator is used for evaluating the feasibility of the generated gait. In the GAOFSF approach, the biped gait is directly given in the joint coordinates. The existence issue of the inversed kinematics solution is thus avoided.

The coordinates, (P_x, P_y), of the ZMP (with reference to the ZMP frame) can be determined as [13,14,24]

$$P_x = \left(\sum_{i=1}^{n} m_i(\ddot{z}_i + g)x_i - \sum_{i=1}^{n} m_i \ddot{x}_i z_i - \sum_{i=1}^{n} I_{iy} \ddot{\Omega}_{iy} \right) \Big/ \sum_{i=1}^{n} (\ddot{z}_i + g)m_i \tag{7.1}$$

$$P_y = \left(\sum_{i=1}^{n} m_i(\ddot{z}_i + g)y_i - \sum_{i=1}^{n} m_i \ddot{y}_i z_i - \sum_{i=1}^{n} I_{ix} \ddot{\Omega}_{ix} \right) \Big/ \sum_{i=1}^{n} (\ddot{z}_i + g)m_i \tag{7.2}$$

where x_i, y_i, and z_i are the coordinates of the centroid of link i; m_i is the mass of link i; I_{ix} and Ω_{ix} are the centroidal moment of inertia and angular displacement, respectively, about the X-axis; I_{iy} and Ω_{iy} are the corresponding parameters about the Y-axis; and g is the acceleration due to gravity. Here, for the planar robot used, only Eq. (7.1) is needed since only motion in the sagittal plane is considered.

For a given set of joint angle trajectories, if the trajectory of the ZMP remains strictly within the area covered by the supporting convex hull of the robot, the given locomotion will be physically feasible and the robot will not topple over while executing the motion. Thus, ensuring that the trajectory of the ZMP remains within a small region of the robot's support polygon is used as one of the key criteria in the objective function for the optimization process.

3.2. Optimization method—genetic algorithm

In order to generate the desired joint angle trajectories for stable walking, a suitable set of coefficients A_i, B_i, C_i and parameters c_h, c_k, t_1, t_2 (refer to Fig. 3b) need to be obtained. t_1 is the instant when the knee of the stance foot starts to lock and t_2 is the instant when the walking phases of the two legs are switched. Because all performance indices can be expressed explicitly, GA[22] provides a very straightforward way to search for the required parameters. This will be discussed in the following sections. The sequence of GA implementation is summarized as follows:

1. Select a fitness function (the goal for the optimization process).
2. Code the parameters to be varied for optimization into genes to form a chromosome.
3. Randomly generate a fixed population of chromosomes and evaluate their fitness values.
4. Apply the reproduction operator to generate a new population of chromosomes with the ones having better fitness values from the previous generation being given higher probabilities of being selected.
5. Randomly choose the mating gene pair and the crossover site. Apply the crossover operator to generate the new pair of chromosomes. Apply the mutation operator.
6. Repeat Step (5) until a fixed number of generations has been generated.

In the demonstration example used here, it was found, through experimentation, that a value for n in both Eqs. (6) and (7.1) as low as 5 gives good performance. This value was thus used. In this case, there will be altogether 19 parameters to be determined. These parameters are coded in a chromosome, which has 19 genes. The chromosome representation can be in binary, integer, or real numbers. Here, the real number representation[22] was adopted which, from experiments performed, is more efficient than the other representations. It takes about 1 min on a Pentium 4, 2.8 GHz computer to find out the solution that fulfils all motion requirements.

The next step is to implement appropriate GA operators, which will yield successful outcomes for the optimization process. The GA operators usually include selection, crossover, and mutation. The properties and parameters given to the GA operators for this work are given in the Appendix (Tables A1–A3).

3.3. Fitness function

One of the most important steps of GA is the formulation of the fitness function. To achieve a natural walking gait while maintaining adequate walking stability, an objective function (to be minimized) is formulated as

$$f_T = w_1 f_1 + w_2 f_2 + w_3 f_3 + w_4 f_4 \tag{8}$$

where w_1, w_2, w_3, and w_4 are weighting factors, and f_1 is the sum of the distances from the ZMP to the center of the

https://doi.org/10.1017/S026357470700344X Published online by Cambridge University Press

support polygon over a walking step

$$f_1 = \sum_{i=1}^{m} |P_i Q| \tag{9}$$

where P_i is the ZMP position at the ith sampling instant; Q is the position of the center of the support zone, and m is the total number of samples in one walking step.

f_2 is the standard deviation of the distance from the ZMP to the average ZMP position

$$f_2 = \sqrt{\frac{(x_1 - \bar{x})^2 + (x_2 - \bar{x})^2 + \cdots (x_m - \bar{x})^2}{m}} \tag{10}$$

where $x_i = |P_i Q|,\ i = 1, 2, \ldots, m$ and $\bar{x} = (1/m)\sum_{i=1}^{m} |P_i Q|$. With f_1 and f_2, the ZMP is aimed to be located in a specific area, which is as small as possible. They also reduce the chance of having a sudden change in the ZMP position.

f_3 is the standard deviation of the trunk velocity from the resulting average velocity over a walking cycle

$$f_3 = \sqrt{\frac{(v_1 - \bar{v})^2 + (v_2 - \bar{v})^2 + \cdots (v_m - \bar{v})^2}{m}} \tag{11}$$

where v_i, $i = 1, 2, \ldots, m$, is the trunk's velocity at the ith sampling instant and $\bar{v}$ is the resulting average trunk velocity over a walking cycle.

$$f_4 = \text{swing foot ground strikes velocity},\ v_s \tag{12}$$

which prevents any instability from larger ground impacts on landing.

In addition to the above four components of the objective function to be minimized, there are six penalty functions for motion constraints to ensure a valid and natural walking motion. Motion constraints work differently from the previous motion objectives. For a motion constraint, there is no penalty if the constraint is not violated. A penalty is only imposed when the motion violates the constraint. The six motion constraint penalty functions are described below.

s_1 constrains the ZMP to be within the support polygon, with $P_i Q \subseteq [-L_1,\ L_2]$ (according to the ZMP coordinate frame origin O) where L_1 is the distance of the heel from the ankle joint and L_2 is that of the toe from the same.

$$s_1 = \max\left(\left(|P_i Q| - \frac{1}{2}L_f\right),\ 0\right) \tag{13}$$

where $L_f = L_1 + L_{2s}$ is the length of the robot foot.

s_2 constrains the swing height to be above a specified minimum value except the phase-switch moment so that the swing foot does not hit the ground prematurely or drag on the ground.

Let m be the number of the sampling instances within one walking step; d_1 and d_2 be the sums of the differences between the desired swing height and the actual height for one walking step; H_r and H_l be the length projections of the right and the left leg, respectively, to the vertical plane with respect to the terrain surface; and $H_{\min}$ be the minimum swing height. With this constraint, although the swing height cannot be always above the minimum height, the problem of the swing foot dragging on the ground for a long time will be avoided.

$$\begin{aligned}
&\text{for} \quad i = 1 : m \\
&\quad \text{if}(t(i) <= t_2) \\
&\quad d_1 = d_1 + \max((H_r - H_l - H_{\min}), 0); \\
&\quad \text{else if}(t(i) > t_2) \\
&\quad d_2 = d_2 + \max((H_l - H_r - H_{\min}), 0); \\
&\text{end} \\
&s_2 = d_1 + d_2
\end{aligned} \tag{14}$$

s_3 constrains the trunk's velocity to be always positive

$$s_3 = \max(-v_i,\ 0) \tag{15}$$

where v_i is the trunk velocity, and the max function is taken over all the sampling instances for the walking step.

s_4 constrains the swing foot's velocity to be always positive except during the short time period before swing foot touchdown

$$s_4 = \max(-v_f,\ 0) \tag{16}$$

where v_f is the swing foot velocity, and the max function is taken over all the sampling instances for the walking step.

s_5 constrains the deviation of the step length to be within a small specified value

$$s_5 = |L - L_0| \tag{17}$$

where L and L_0 are the actual and the desired step lengths, respectively. It can be regarded as a soft motion constraint.

s_6 constrains the deviation of the foot's touch-down instant, t_d, from the planned phase switching time, t_2, to be within a small specified value

$$s_6 = |t_2 - t_d|. \tag{18}$$

Based on these constraints, a penalty function is defined as

$$P = \sum_{i=1}^{6} p_i s_i \tag{19}$$

where $p_i,\ i = 1, \ldots, 6$, are assigned penalty weighting factors.

Using Eqs. (8) and (19), the fitness function for the GA algorithm is established as

$$F = \begin{cases} 0, & \text{if } \sum_{i=1}^{n} |A_i| = 0 \quad \text{or} \quad \sum_{i=1}^{n} |B_i| = 0 \\ & \text{or} \quad \sum_{i=1}^{n} |C_i| = 0 \\ C_{\max} - f_T - P, & \text{otherwise} \end{cases}. \tag{20}$$

https://doi.org/10.1017/S026357470700344X Published online by Cambridge University Press

Table II. Two flat-terrain walking examples.

	Example 1	Example 2
Step length	0.33 m	0.28 m
Walking speed	0.45 m/s	0.37 m/s

The first expression of Eq. (20) is used to avoid the possible situation of standing still which can give a very good performance on the ZMP-based stability objective. The parameter $C_{\max}$ is chosen to be as small as possible in order to have a better differentiation among various possible solutions. However, it should also be such that the fitness value for most, if not all, possible solutions are positive. Suitable values are chosen by trial and error.

In some cases, it is still possible for the fitness values to be negative, indicating a very weak chromosome. However, it is also possible for a bad chromosome to evolve to be better and better. To cater to these possibilities, if the fitness value for a chromosome works out to be negative, a small value is assigned to it considering a small probability of survival. If it continues to be weak after crossover and mutation, it will be discarded eventually.

In selecting the values for the weight factors w_i and p_i, consideration was given to balance all objectives and constraints, usually through estimating f_1 to f_4 and s_1 to s_6 values of a normal performance and then estimating the weight factors to make them almost equally important.

4. Gait Patterns Generated by GAOFSF

The aforementioned GAOFSF approach was applied to the planar biped illustrated in Fig. 2, with the geometrical and inertial properties as given in Table I. The TFS, with $n = 5$, was used for the joint angle trajectories described in Eqs. (5) and (6). Walking gaits for flat-terrains (two examples), one with a 10° up-slope and another with a 10° down-slope, were then generated.

4.1. Flat-terrain walking

To achieve a natural human-like gait, do not take the small stance knee angle change as significant, the knee joint angle offset value, $c_k = 0$. The appendix gives the set of parameters used for the GA initialization and the weights for the objective and penalty functions. The step lengths and walking speeds used for the two flat-terrain walking examples are shown in Table II.

The format of the chromosome is set as $[A_i, B_i, C_i, c_h, c_k, t_1, t_2]$. The chromosome solutions, x_1 and x_2, obtained for flat-terrain walking Examples 1 and 2, respectively, are

$$x_1 = [0.277 \quad -0.087 \quad 0.022 \quad -0.008 \quad -0.000 \quad -0.397 \quad -0.118 \quad -0.024 \quad -0.017 \quad -0.006 \quad 0.457 \quad 0.200 \quad -0.038 \quad -0.077 \quad -0.046 \quad -0.036 \quad 0.000 \quad 0.050 \quad 0.44]$$

$$x_2 = [0.238 \quad -0.057 \quad 0.012 \quad -0.004 \quad 0.0003 \quad -0.356 \quad -0.043 \quad 0.042 \quad 0.004 \quad -0.003 \quad 0.469 \quad 0.074 \quad -0.050 \quad 0.008 \quad -0.017 \quad -0.021 \quad 0.000 \quad 0.065 \quad 0.47]$$

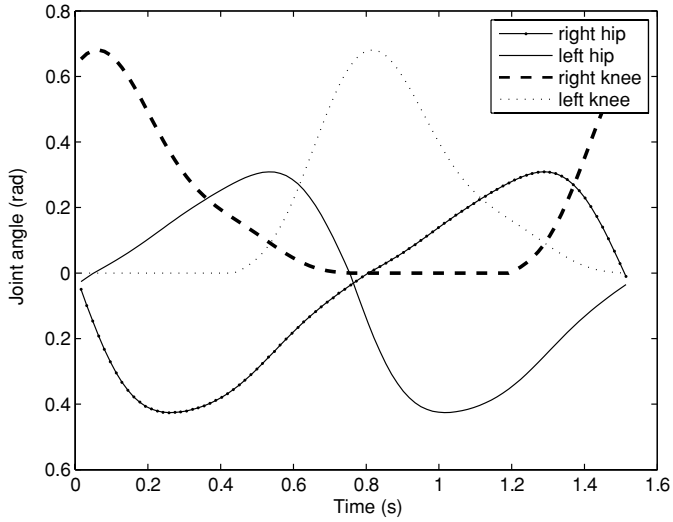

Fig. 4. Generated joint angle trajectories (Example 1, flat terrain).

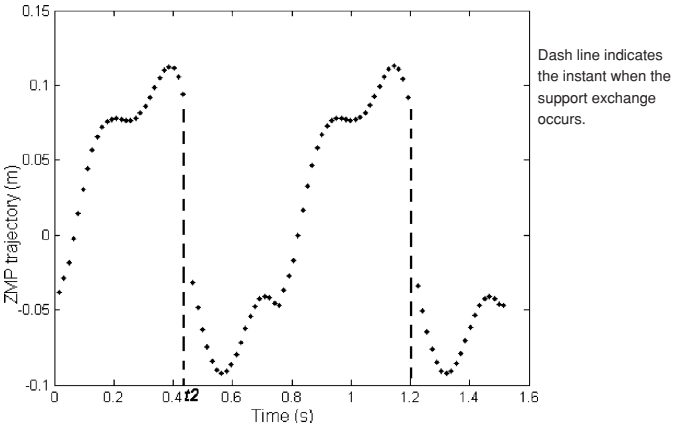

Fig. 5. ZMP trajectory (Example 1, flat terrain).

For the above two examples, $\omega_h = 4.28$ and $\omega_h = 4.15$, respectively. The value of $C_{\max}$ used for the GA is 1400 and the fitness function values for the two solutions are 1287 and 1309, respectively, indicating good optimization performances. What follows will show that the generated gaits results are in accordance with the objectives and constraints.

From the solution obtained for Example 1, the corresponding hip and knee joint angle trajectories, generated using the TFS, are shown in Fig. 4. Figure 5 shows the trajectory of the ZMP for one walking cycle and Fig. 6 shows the position of the centroid of the trunk versus time. It can be observed that the ZMP trajectory is confined within the safe area (−0.08, 0.12) m of the footprint (−0.1, 0.2) m, which is fair enough for such a step length and speed walking for a robot of the size shown in Table I. From Fig. 6, it is observed that an even walking speed of 0.45 m/s has also been achieved via the estimation of the inclination of the position–time plot. Fig. 7 shows the difference $(f_l - f_r - h_r)$ between the lengths of the vertical projections of the left and the right legs. The results show that the swing foot is kept above the ground during the swing phase. The instant of swing leg touchdown occurs at $t_d = 0.44$ s (with $f_l = f_r$; $h_r = 0$ for flat-terrain). This is equal to t_2 in the x_1 chromosome. Checking whether t_d, the touch down

https://doi.org/10.1017/S026357470700344X Published online by Cambridge University Press

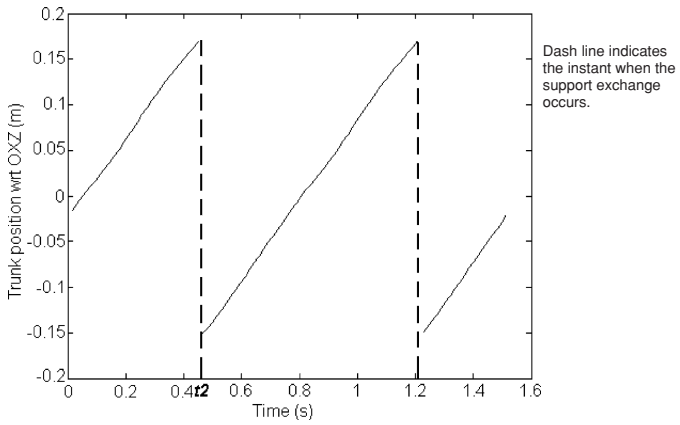

Fig. 6. Trunk speed seen from the inclination (Example 1, flat terrain).

instant of the swing foot, is equal to t_2, the planned switching instant between the two legs, is important for the validity of the calculation of the ZMP trajectory. Referring to Fig. 7, if f_l and f_r are the vertical projections of the left and right legs, respectively, and h_r is the vertical height of the slope at the point above the stance foot (for flat-terrain walking, h_r is set to be zero), then the following relationship applies

$$\begin{cases} f_l \geq f_r + h_r & (t \leq t_2) \quad \text{left leg is stance leg} \\ f_r > f_l + h_l & (t > t_2) \quad \text{right leg is stance leg} \end{cases}$$

Figure 8 shows the stick diagram of the final resulting motion pattern. From the motion data obtained, the swing foot touchdown strike velocity $[v_x, v_z]$ is found to be $[0.15, -0.2]$ m/s. The resulting ground impact is found to be acceptable from the subsequent dynamic simulations to be discussed in a later section. The step length is found to be equal to 0.327 m, very close to the set target.

The resulting motion obtained for Example 2 is illustrated in Figs. 9–11. Due to a smaller step length, the ZMP is as expected confined to a smaller range compared to Example 1. The swing foot touchdown strike velocity is found to be $v_x = 0.12$ m/s and $v_z = -0.2241$ m/s; the step length to be 0.27062 m; the average walking speed to be around 0.36 m/s, and the first foot touchdown instant to be $t_d = 0.47$ s, which is also equal to t_2 in the GA solution.

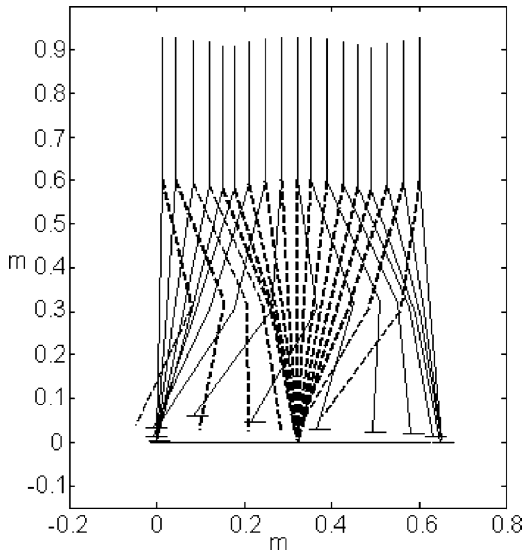

Fig. 8. Stick diagram of the motion (Example 1, flat terrain).

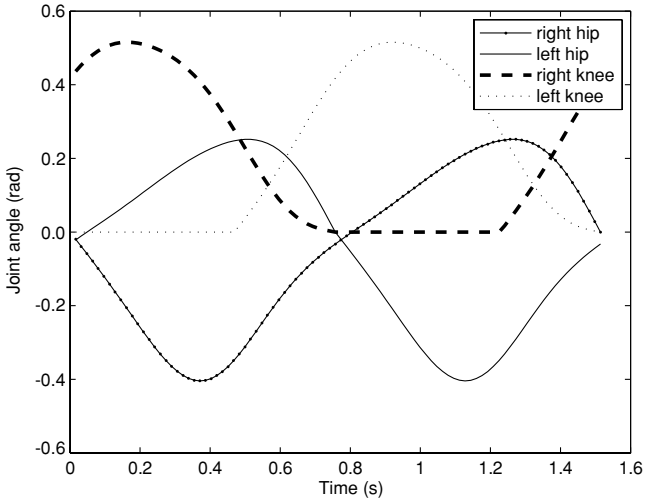

Fig. 9. Generated joint angle trajectories (Example 2, flat terrain).

Therefore, the results obtained for those two examples of flat-terrain walking confirm that the proposed approach can be used to synthesize reliable and overall optimal (in the

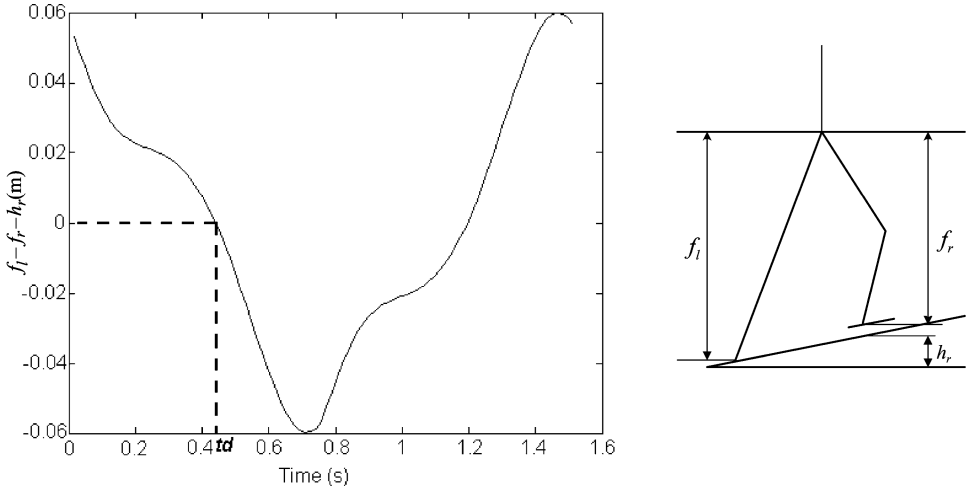

Fig. 7. (a) $f_l - f_r$ (m) versus time. (b) f_l, f_r and h_r illustrations.

https://doi.org/10.1017/S026357470700344X Published online by Cambridge University Press

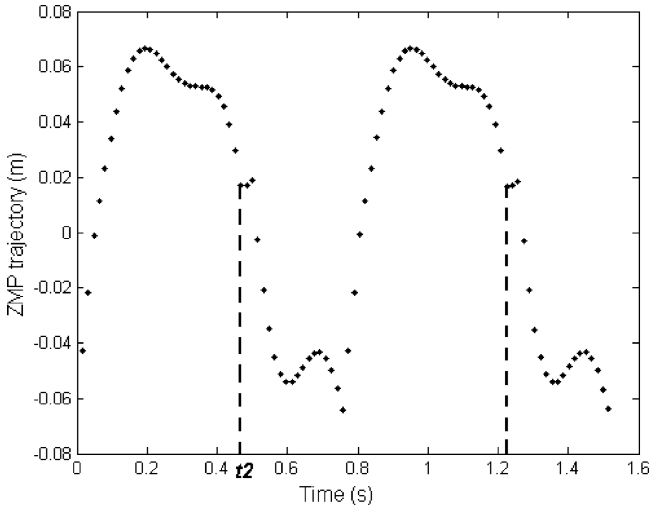

Fig. 10. ZMP Trajectory (Example 2, flat terrain).

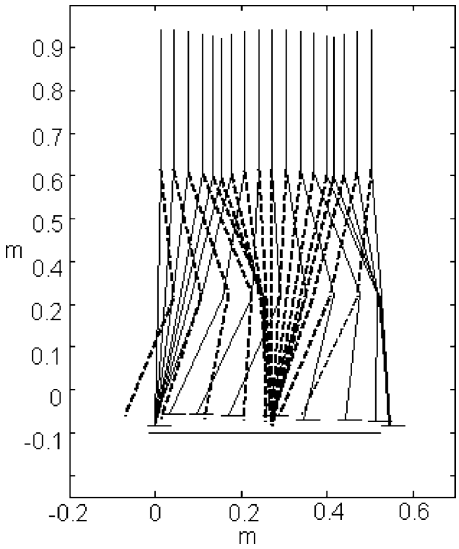

Fig. 11. Stick diagram of the motion (Example 2, flat terrain).

sense of objective functions) trajectories with stable human-like walking gaits.

From these solutions, which resembled the typical hip and knee joint trajectories and satisfied all performance indices, it can be noted that coefficients for all the fifth-order term in the TFS are very small in comparison to that for the first term. Therefore, it shows that the fifth-order TFS used is sufficient for the gait synthesis and higher-order TFS are not significantly necessary. To demonstrate the generality of the proposed GAOFSF approach, it is applied to generate gaits for walking on slopes or on stairs. The results for these are presented in the following sections.

4.2. Slope-terrain walking

The "footprint" in the case of inclined terrain walking is the projection of the footprint of the stance foot onto the horizontal plane.

In the first slope walking example, the GAOFSF approach was used to generate the joint trajectories for the robot to walk up a 10° slope. The desired step length is set to 0.26 m and the average walking speed along the horizontal plane is

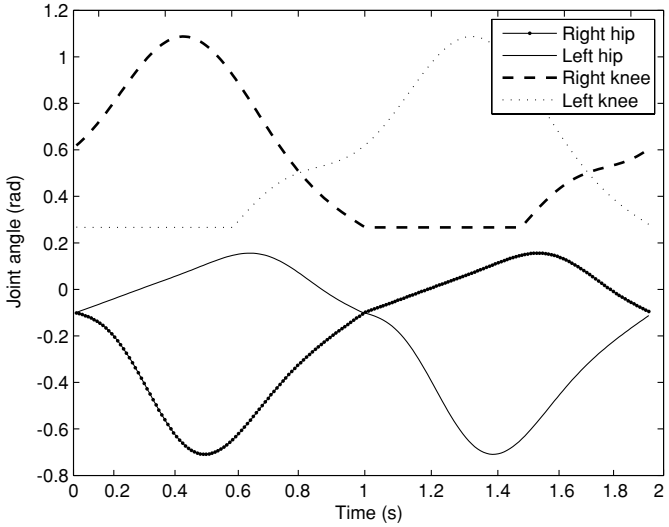

Fig. 12. Generated joint angle trajectories (up-slope).

set to 0.27 m/s ($\omega_h = 3.2623$). The GA parameters are shown in the Appendix.

The best chromosome, $[A_i,\ B_i,\ C_i,\ c_h,\ c_k,\ t_1,\ t_2]$, corresponding to a fitness value of 2860 and with $C_{\max} = 3000$, was found by GA to be

$$x_{\text{up}} = [0.222 \quad -0.041 \quad -0.011 \quad 0.014 \quad -0.005$$
$$-0.500 \quad -0.035 \quad 0.097 \quad 0.039 \quad 0.004$$
$$0.650 \quad -0.096 \quad -0.087 \quad 0.085 \quad 0.024$$
$$-0.144 \quad 0.267 \quad 0.001 \quad 0.540].$$

Figure 12 shows the resulting joint angle trajectories, which are similar in form as those shown in Fig. 3. Figure 13 shows the trajectory of the ZMP. It is clear that the ZMP trajectory is well restricted within the safe area $(-0.0985,\ 0.197)$ m of the footprint. The resulting walking speed is 0.265 m/s and the swing foot strike velocity, $[v_x,\ v_z]$, is found to be $[0.042,\ -0.28]$ m/s which will not cause an unduly large ground impact as confirmed by the subsequent dynamic simulation. The step length obtained is 0.261 m, which is also very close to the target value. The actual strike instant,

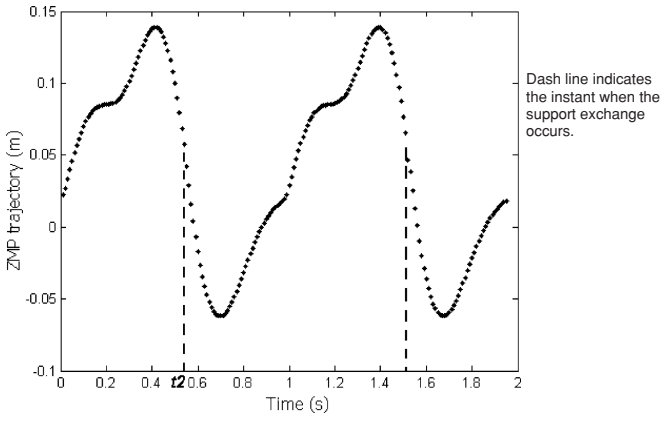

Fig. 13. ZMP trajectory (up-slope).

https://doi.org/10.1017/S026357470700344X Published online by Cambridge University Press

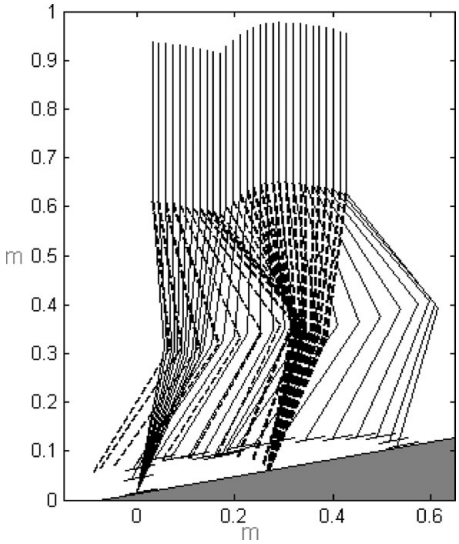

Fig. 14. Stick diagram of 10° up motion.

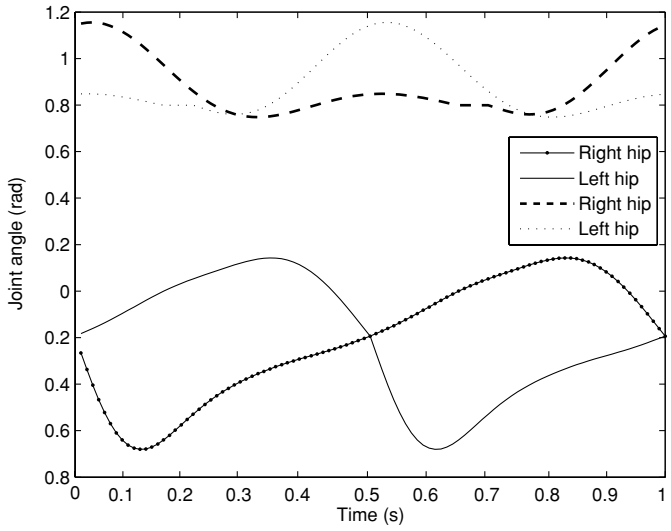

Fig. 15. Generated joint angle trajectories (down-slope).

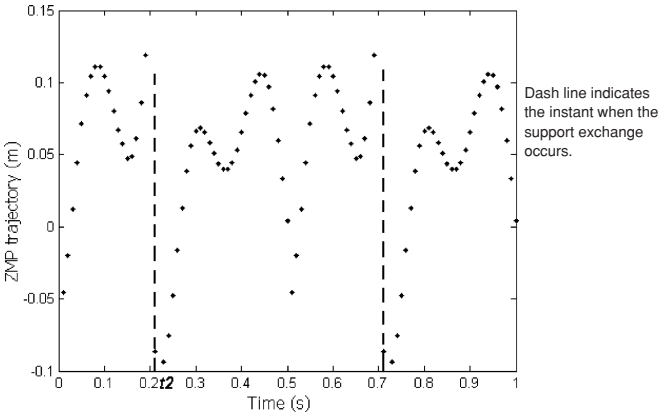

Fig. 16. ZMP trajectory (down-slope).

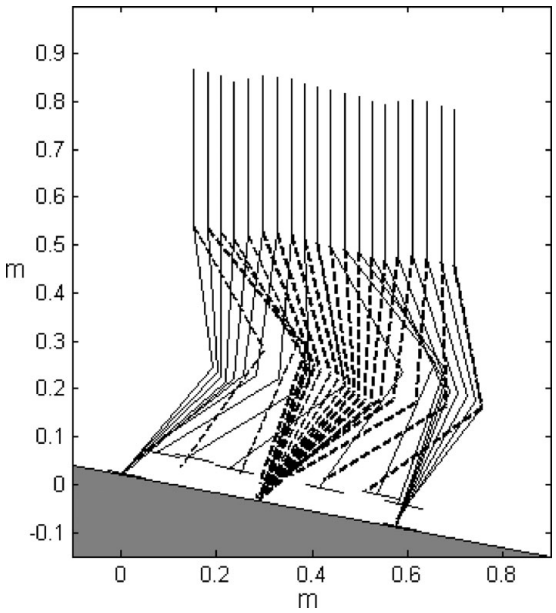

Fig. 17. Stick diagram of the motion (10° down-slope).

at $t = 0.54$ s, is the same as t_2 in the solution. Figure 14 shows the stick diagram of the locomotion.

The second case involved walking down a 10° slope. The step length was set to 0.35 m and the average walking speed to 0.6 m/s ($\omega_h = 2\pi$). The GA parameters used are shown in the Appendix. The best chromosome obtained by GA, in the form of $[A_i, B_i, C_i, c_h, c_k, t_1, t_2]$, with $C_{\max} = 3000$ and corresponding to a fitness value of 2935, is

$$x_{\text{down}} = [0.312 \quad -0.076 \quad 0.018 \quad -0.005 \quad -0.004 \quad -0.327 \quad -0.190 \quad -0.096 \quad -0.031 \quad -0.009 \quad 0.144 \quad 0.118 \quad -0.007 \quad -0.114 \quad -0.033 \quad -0.194 \quad 0.799 \quad 0.147 \quad 0.220].$$

Figure 15 shows the resulting joint angle trajectories. Figure 16 shows that the ZMP trajectory is also well restricted within the safe area of the footprint. For this motion, the swing foot strike velocity $[v_x, v_z]$ is $[-0.15, -0.5]$ m/s, respectively. The actual step length is 0.35 m and the walking speed is about 0.625 m/s. The first leg strike instant is at $t = 0.21$ s, which is also very close to t_2 in the GA solution. The resulting motion is shown in Fig. 17.

The results obtained for flat-terrain, up-slope, and down-slope motions show that the GAOFSF is effective and uniform in generating gaits that meet all the constraints and which maximize the objectives. The resulting motions are feasible and have similar forms as in the natural human gait.

From the results, it is noted that although the general shapes of the joint angle trajectories obtained as similar in form to that shown in Fig. 3b, there is a significant difference in the value of t_1, the instant when the stance knee starts to lock for the different slopes. For both flat terrains and up-slope walking, t_1 is negligible but for down-slope walking, the period from t_0 to t_1 is quite significant. This shows that, in the latter case, the stance knee joint is locked for only a very short duration or may not be locked at all.

In the following section, the dynamic simulations for the generated stable locomotion with human-like gaits will be presented.

https://doi.org/10.1017/S026357470700344X Published online by Cambridge University Press

5. Dynamic Simulation of Generated Gaits

For the joint angle trajectories generated by GAOFSF, dynamic simulations were then performed using the seven-link bipedal robot modeled as Table I. The simulation software used is Yobotics!.[29] In this simulation environment, the dynamics of the robot, based on Newton–Euler equations, are performed automatically and the user only needs to set up the robot structure based on a high level constructor and the ground contact behavior. The latter is essentially based on a spring-damper model which has both horizontal and vertical components. In the simulation, Yobotics! models the ground properties and gives the sensed dynamic information like velocity, acceleration, and ground reaction forces directly.

The hip and knee joints' trajectories are generated by the GAOFSF approach. The swing ankle joint trajectory is generated in real-time by using the fact that the swing foot is desired to be parallel to the ground at all time. The stance ankle joint trajectory is generated in real-time by using the fact that the body pitch is desired to be zero at all times. To further ensure a smooth switching of the stance phase between the legs, the ankle joint was loosened at the point when either the toe or heel touches the ground. This ensures that the swing foot is parallel to the ground at touchdown and, thereafter, as the stance foot it is always compliant and in full contact with the ground. This makes the ZMP criterion always applicable as a check on gait feasibility. On the other hand, if the actual motion gets the right track as the planned one, the stance foot is not supposed to flip during the motion. For hip and knee joint control, local PD controllers are used, for example, the stance hip joint control law is given as

$$\tau_{sth} = K_{sth}\left(\theta^d_{sth} - \theta_{sth}\right) + D_{sth}\left(\dot{\theta}^d_{sth} - \dot{\theta}_{sth}\right) \qquad (21)$$

where τ_{sth} denotes the stance hip joint torque; K_{sth} and D_{sth} are the proportional and derivative gains, respectively; θ_{sth} and θ^d_{sth} are the actual and desired stance hip angles, respectively; and $\dot{\theta}_{sth}$ and $\dot{\theta}^d_{sth}$ are the actual and desired stance hip angular velocities, respectively.

There are three reasons to choose PD control to test the GAOFSF. Firstly, if PD control can achieve the desired motion well, the planned motion is very confident to be achieved by other more complicated nonlinear controllers. Secondly, in the biological sense, it is said that PD controller can achieve the muscular motions well enough.[30] Lastly, with a properly designed high-level, automatic, rhythmic step length and pattern adjustment according to the real-time information (i.e., trunk CG position), the tracking accuracy is a secondary factor.

To further prove the proposed motion generation method GAOFSF mimics human-like patterns, the ground reaction forces were investigated. Here, the flat-terrain walking is taken to give a comparison with real human walking recorded by VICON system. Figure 20 shows the measured orientation and the magnitude of reaction force in human walking using the VICON system.

The reaction forces (shear force and vertical reaction force) of two flat-terrain walking examples are acceptable,[31] considering the robot weight (Figs. 18 and 19). The lack of visible force impact of the end of support phase, similar to the human gait, suggests there is no obvious dynamic impulse

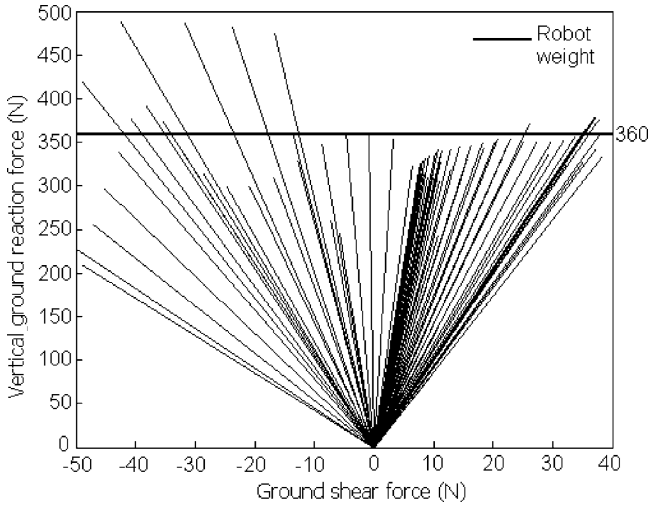

Fig. 18. Ground reaction force of flat-terrain walking 1.

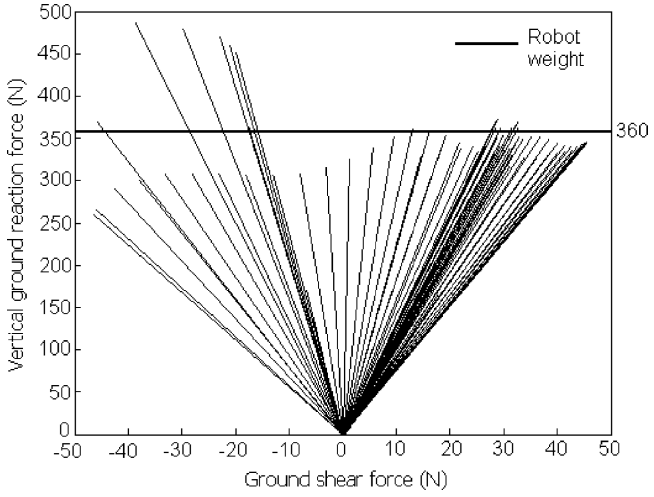

Fig. 19. Ground reaction force of flat-terrain walking 2.

to push the biped. Referring to Figs. 18 and 19, the shear forces are negative at first and then becomes positive. This is exactly what is measured in human gaits. The negative part is the braking phase of touching down and the positive part is the motion propulsion phase when the supporting leg pulls the ground to drive the body. The peak value of shear forces is about 15% of body weight, comparable to 16–20% in human walking. For a better illustration of the changing orientation and magnitude of ground reaction force, a human walking experiment are displayed at once with two different timings (dark gray and light gray), shown in Fig. 20. The length of vector is related to its force magnitude. Comparing the orientation and the magnitude of reaction force in human walking, a good coincidence between the generated gaits and the human counterpart is noticed. The force vectors' orientations rotate clockwise with the progress of the support phase. The value of vertical ground reaction force near the body weight mostly during the support confirms that the robot is supported well.

From Figs. 21 and 22, note that the calculated required friction coefficient is small (<0.25). It means that normal surfaces (PCV floor, wooden floor, brick path, asphalt)

https://doi.org/10.1017/S026357470700344X Published online by Cambridge University Press

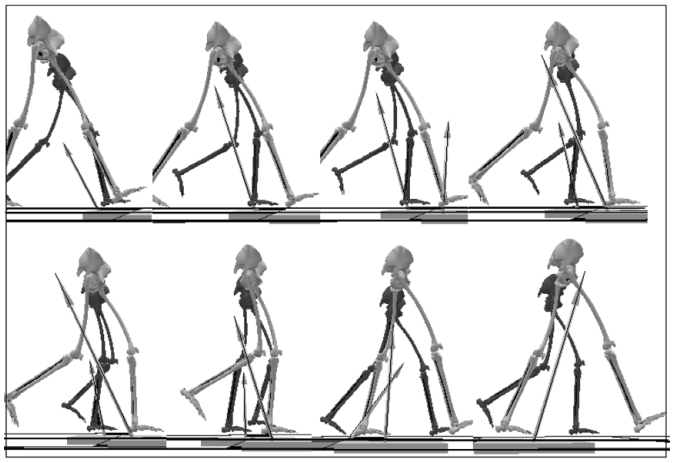

Fig. 20. Orientation and the magnitude of reaction force in human walking.

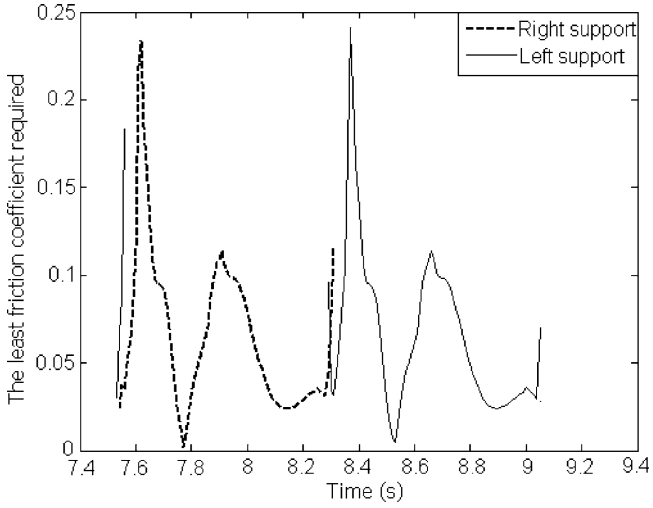

Fig. 21. Required friction coefficient for flat-terrain walking 1.

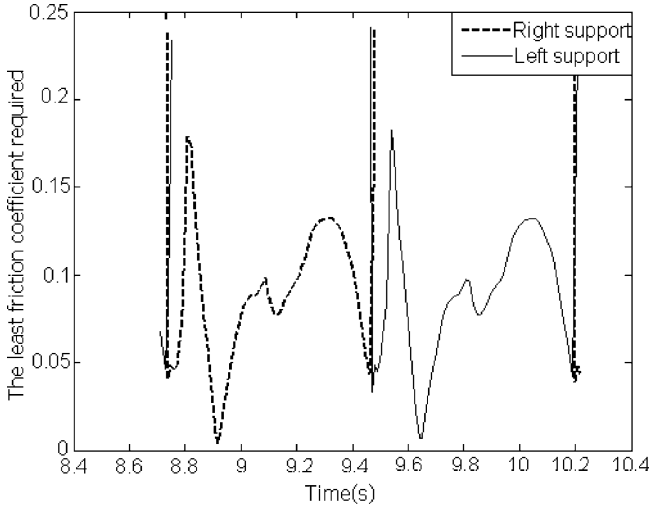

Fig. 22. Required friction coefficient for flat-terrain walking 2.

toward robot feet with shoe-type sole (for those materials friction coefficient ranges from 0.5 to 0.9)[32] can easily satisfy the compensation of shear force without slip. Figures 23 and 24 show the stick diagrams for the corresponding walking motions under the environment of Yobotics!.

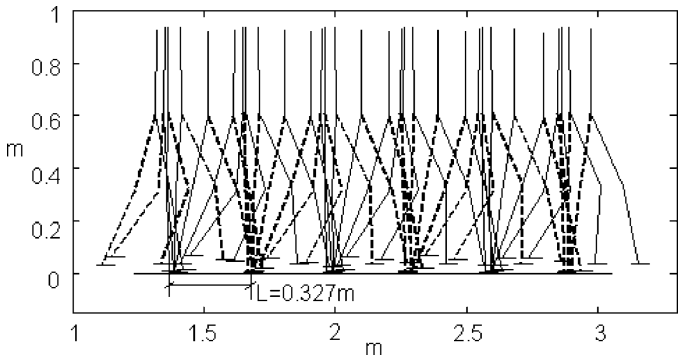

Fig. 23. Dynmic simulation of walking Example 1.

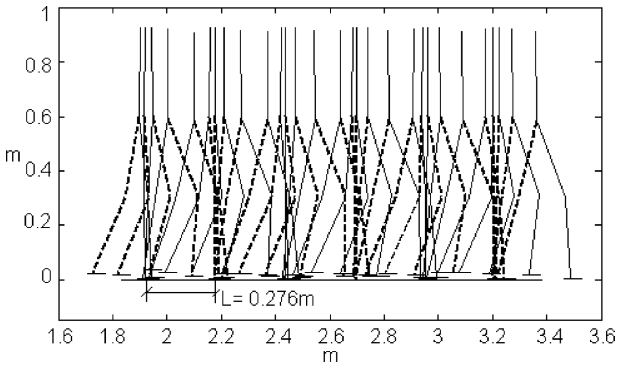

Fig. 24. Dynamic simulation of walking Example 2.

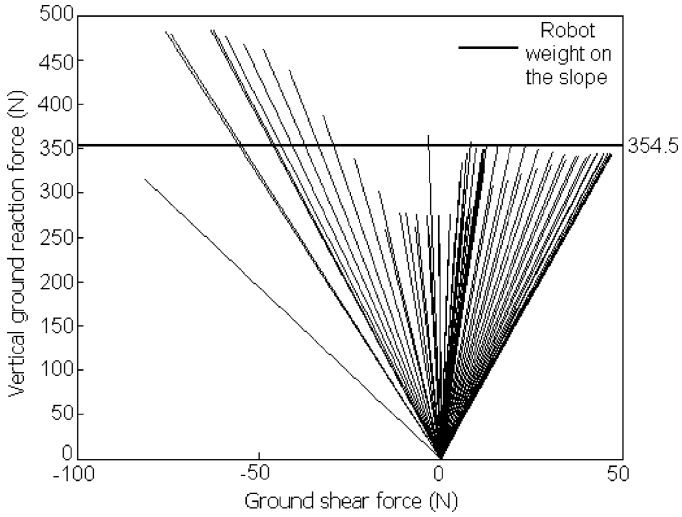

Fig. 25. Ground reaction force of going-up motion.

The up-hill and down-hill motions also have been achieved well comparing the following stick diagrams with Figs. 15 and 19. Similarly, the orientation and magnitude of the ground reaction force for up-slope and down-slope motions are shown in Figs. 25 and 26, respectively. For going down a slope, it is quite natural to have a bigger impact when the swing foot touches the ground comparing with the up-slope or flat-terrain motions.[23] Figures 27 and 28 give the required friction coefficient during the up-slope and down-slope motions, respectively, showing that it is still safe

https://doi.org/10.1017/S026357470700344X Published online by Cambridge University Press

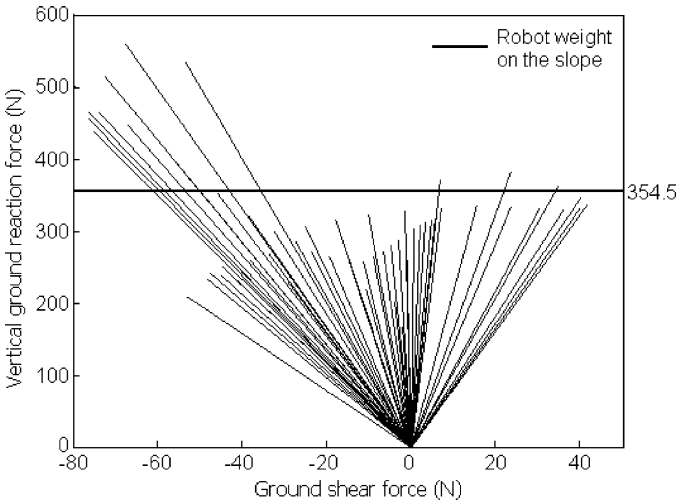

Fig. 26. Ground reaction force of going-down motion.

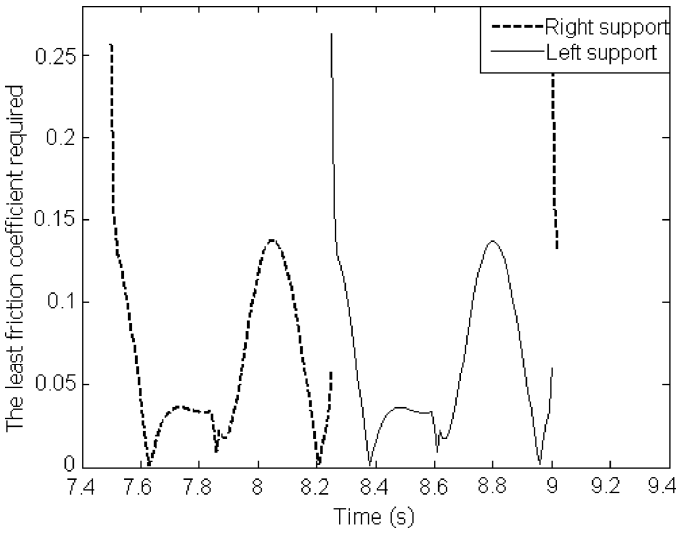

Fig. 27. Required friction coefficient of going-up motion.

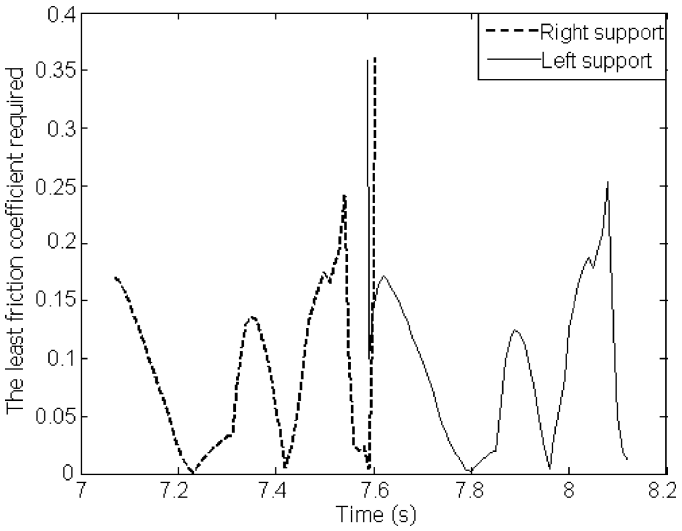

Fig. 28. Required friction coefficient of going-down motion.

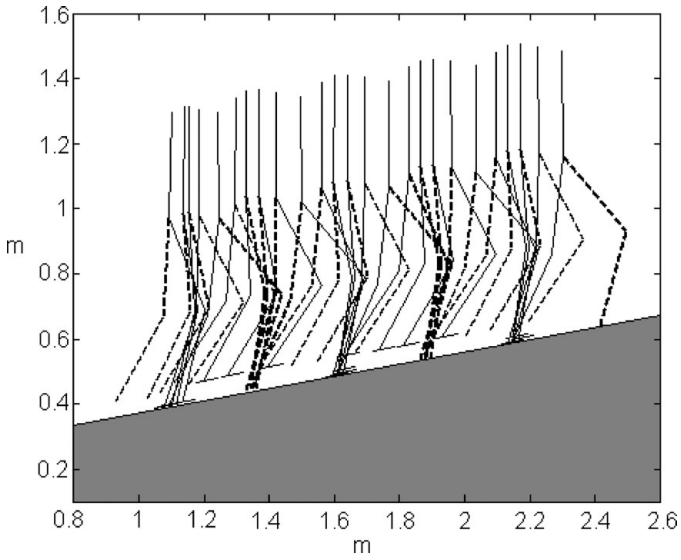

Fig. 29. Stick diagram of actual up motion.

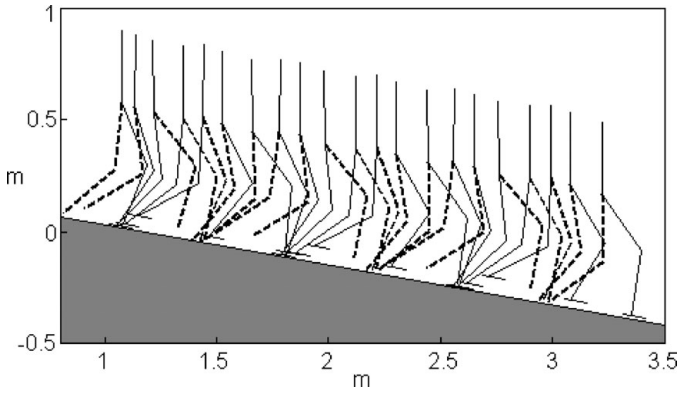

Fig. 30. Stick diagram of actual down-slope motion.

enough to walk on normal grounds. Figures 29 and 30 show the stick diagrams of the up-slope and down-slope walking, respectively.

All the simulation results show that the generated gaits from the GAOFSF approach can be applied directly to the simulated robot without any modification. This implies that the objective function and the motion constraints chosen for the GAOFSF are valid.

6. Gait Adjustment During Walking

Effective control in robotics usually require an online adjustment in the presence of environment change such as disturbance and noise.[33] The foregoing sections present an approach, using truncated Fourier Series (TFS) to represent joint angle and GA to search for optimal trajectories, which has been demonstrated, through dynamic simulations, to be capable of generating stable human-like walking gaits for various specified walking rhythms and for terrains of different specified slopes. In this section, the extent to which the generated gaits can be adjusted, by adjusting certain parameters in the TFS, to accommodate different walking rhythms and terrains of different slopes is discussed. Here, some results are given to show the feasibility of adjusting the parameters of TFS model online.

https://doi.org/10.1017/S026357470700344X Published online by Cambridge University Press

6.1. Step length and rhythm adjustment

From Eqs. (5) and (6), it can be noted that, with the TFS formulation used, the step length can be easily adjusted by changing just the value of the scaling parameter R. The period of the walking cycle can also be simply adjusted by changing ω_h. Both these two parameters directly change the walking speed and gait rhythm of the resulting locomotion.

As noted earlier, changing the step length of the gait can be achieved easily by changing just the value of a single parameter R in the TFS obtained by GAOFSF. In the meantime, with the amplitude of TRS increased, the swing leg lifts higher. It actually also helps to avoid ground obstacles to some degree and resembles what human-beings do. However, there is no guarantee that this will result in stable locomotion. To investigate this, the value of R was varied in the joint angle trajectories obtained earlier by GAOFSF for walking on all the three types of terrains: flat, 10° up-slope, and 10° down-slope. The stability of the resulting gaits was then investigated through dynamic simulations using Yobotics!.

The dynamic simulation results show that different step lengths were achieved and the locomotions were stable and the gaits natural and human-like for all the three types of terrains when the value of R was varied. As an example, the stick diagrams of the resulting motion obtained from the dynamic simulation when R is varied for the down-slope walking are shown in Figs. 31 and 32, for which $R = 0.7$ and $R = 1.1$, respectively. As expected, a big step length also brings a much more obvious swing height.

To investigate the robustness of the trajectories obtained to changes in the stride frequency, similar dynamic simulation experiments were conducted with the value of ω_h varied. Simulation results show that the walking rhythm changes with changes in ω_h and the resulting gaits were confidently stable for variation of ω_h within the range of 2–6. Figures 33 and 34 are stick diagrams illustrating the locomotion obtained for $\omega_h = 2$ and $\omega_h = 6$, respectively. It is noted that these

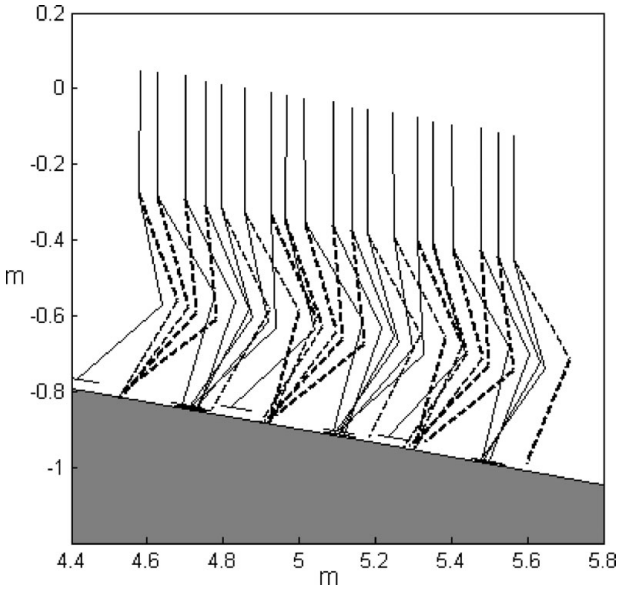

Fig. 31. Down-slope walking with $R = 0.7$.

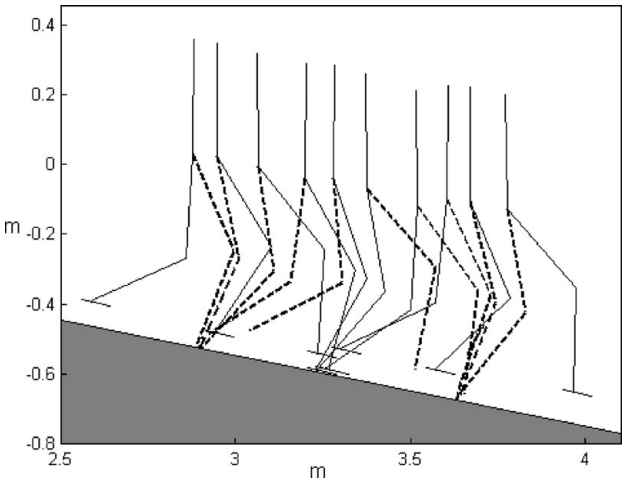

Fig. 32. Down-slope walking with $R = 1.1$.

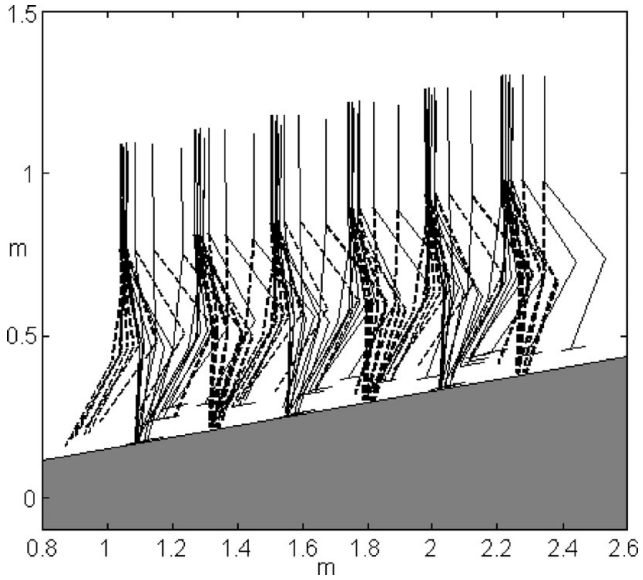

Fig. 33. The slowest walking with $\omega_h = 2$.

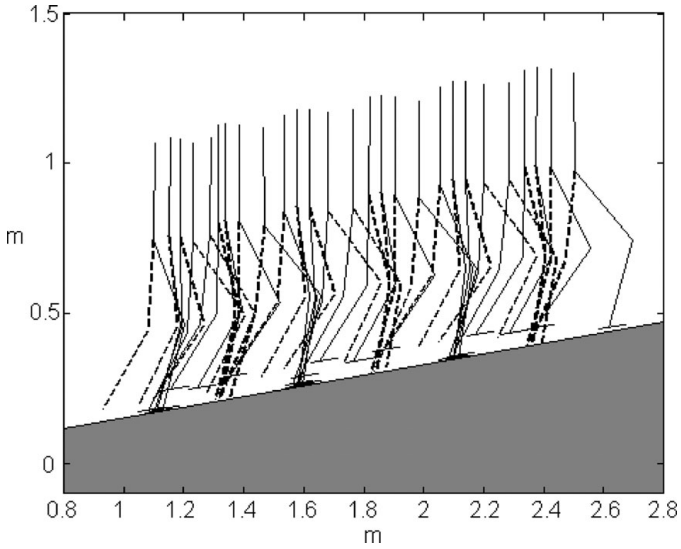

Fig. 34. The fastest walking with $\omega_h = 6$.

https://doi.org/10.1017/S026357470700344X Published online by Cambridge University Press

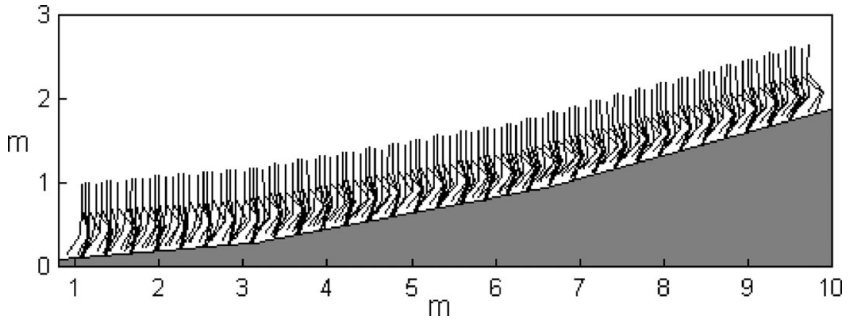

Fig. 35. Walking on an up-slope with changing gradient.

values are 61% and 184% of the value of ω_h used in the solution obtained by GAOFSF.

6.2. *Walking on different slopes*

The gaits obtained by GAOFSF for walking on slopes were optimized for stable walking only for a slope with a specific gradient. The gaits obtained earlier, for example, are optimized for stable walking on a terrain with a gradient of 10° up-slope and 10° down-slope. Here we investigate how the TFS obtained by GAOFSF can be adjusted for stable walking on slopes with different gradients.

From dynamic simulation experiments, it is found that by appropriately changing only the values of c_h and c_k in the TFS of Eqs. (5) and (6), stable gaits can be obtained for walking on different slopes. The rules for changing these two parameters are as follows (the derivation of those rules will be discussed in the sequent report)

$$\begin{cases} c_h = 6.3e^{-005}\alpha^3 - 1.2e^{-003}\alpha^2 - 1.8e^{-002}\alpha + 0.039 \\ c_k = -1.2e^{-004}\alpha^3 + 2.5e^{-003}\alpha^2 + 2.6e^{-002}\alpha + 0.12 \end{cases}$$

for up-hill motion adjustment

$$\begin{cases} c_h = 1.7e^{-005}\alpha^3 + 3.6e^{-004}\alpha^2 + 3.9e^{-003}\alpha - 0.22 \\ c_k = 1.2e^{-005}\alpha^3 - 4.5e^{-005}\alpha^2 - 2e^{-002}\alpha + 0.69 \end{cases}$$

for down-hill motion adjustment

where α is the gradient of the slope terrain. Figure 35 shows the stick diagram obtained from dynamic simulations for stable walking up a sloped terrain for which the gradient changes from +4° to +11° to +15°.

Figure 36 shows the corresponding stick diagram for walking down a slope with the gradient changing from −15° to −7° to −2°.

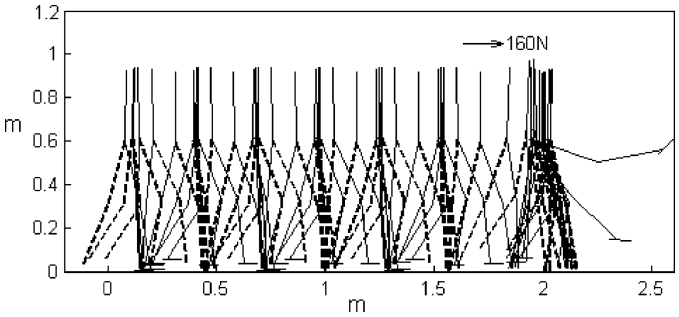

Fig. 37. Instability resulting from an external impulsive disturbance.

7. A TFS-Based Approach for Gait Generation in a Changing Environment

As can be seen from the foregoing sections, the TFS model for the joint angles generated by the GAOFSF approach can be easily adjusted, through the adjustment of only a few parameters, to accommodate for a range of step lengths, stride frequencies, and different slopes, and still maintain a stable gait. Depending upon the range of step lengths and stride frequencies desired, more than one set of TFS could be generated by GAOFSF and stored as reference sets, each for a different range of step lengths and stride frequencies. Because of the robustness of the generated TFS to changes in both step lengths and stride frequencies as discussed in the previous section, only a few sets will be needed for any particular biped. Depending upon the step length and stride frequency desired, and the slope of the terrain encountered, the appropriate set of TFS with suitable values of R, ω_h, c_h, and c_k can then be used to generate the necessary joint angle trajectories for the gait required.

The approach can also be used effectively to achieve stable walking in an uncertain external environment if suitable

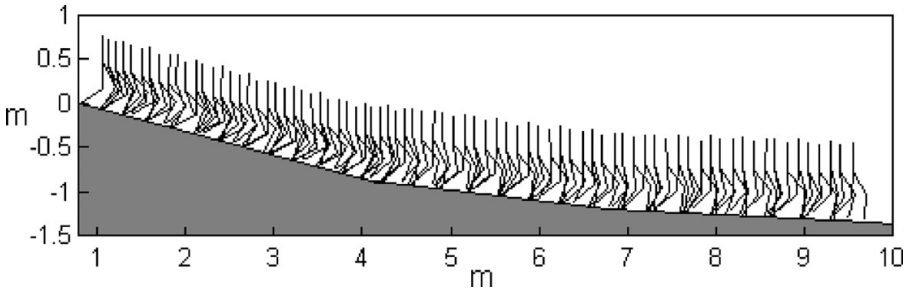

Fig. 36. Walking on a down-slope with changing gradient.

https://doi.org/10.1017/S026357470700344X Published online by Cambridge University Press

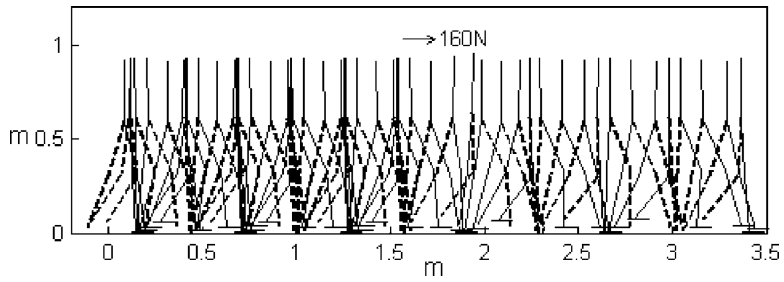

Fig. 38. Maintaining stability by increasing walking rhythm ω_h.

sensing of the external environment and perturbations are available. For example, if the robot should experience an external applied force which requires it to speed up in order to maintain stable walking, this could readily be achieved by a simple upwards adjustment to both R and ω_h in the TFS, thereby increasing its step length as well as stride frequency.

As an example, a dynamic simulation was performed to study the effect of the application of an external impulse, in the form of a 160 N force acting for 0.1 s, on a robot walking on a flat terrain. If the walking rhythm is not adjusted to accommodate for this external impulse, the robot's rhythmic motion will be disrupted resulting in instability. The stick diagram obtained from the dynamic simulation is as shown in Fig. 37.

However, if in response to the external impulsive force, the walking pace is appropriately increased, the robot can maintain balance and continue with its stable walking. Figure 38 shows the results of the dynamic simulation of such an example. In this case, the same impulsive force was applied but this time, in response, the stride frequency, ω_h, was increased to 5 from 3.2 and the step length increased from $R = 1$ to $R = 1.1$.

8. Conclusions

In this paper, the GAOFSF approach using a truncated Fourier Series (TFS) to model the joint angle trajectories for a biped is proposed. Genetic Algorithm (GA) is used to search for an optimal set of trajectories according to some specified objective functions and constraints. The approach was applied for generating stable gaits for a seven-link biped walking on flat terrains, and on terrains with different slopes. Dynamic simulations using the generated gaits demonstrate the viability of the approach for generating stable gaits.

The proposed approach, using TFS to represent the joint angle trajectories, has several advantageous features. It does not require inverse kinematics, thus avoiding the attendant singularity problem. The approach is general and can be readily applied to different motions such as marching or braking to standing still by motion descriptions, and can be easily applied to a biped with different geometrical and inertial properties because the computation cost of the offline GA is low, taking only a couple of minutes at most for a motion result using a normal equipped Pentium IV PC. The generated gaits captured some human walking features. Through changing the value of only one parameter in the TFS, stable gaits with different step lengths and stride frequencies can be readily generated. As has been demonstrated through dynamic simulations, the TFS representation also proved to be robust to changes in step lengths and stride frequencies. The gaits generated remained stable even for fairly obvious changes in both step length and stride frequency. The TFS can also be readily adjusted, by changing the values of only two parameters, to produce stable gaits for walking on slopes with different gradients.

With the ease with which TFS can be adjusted to produce stable gaits with different step lengths, stride frequencies, and for slopes with different gradients, the approach lends itself readily for the generation of stable gaits which can adapt to changes in the terrain and in response to external disturbances. To enable stable walking on terrains with changing slopes, sensors giving estimates of the slopes will be necessary. To adapt to external disturbances and uncertainties and to maintain stable walking, some means of sensing and estimation of the dynamic state of the robot will be necessary in order to determine the required optimal step length and stride frequency. This is the subject of current research, extending the application of this approach. Furthermore, future work will illustrate the supervisory control giving reasonable stride frequency and step length automatically when walking on a rough terrain or under perturbations. Moreover, our aim is also to extend the method to the 3D, not only planar model, and to analyze more in detail about the motion synchronization between the other body links such as trunk, upper limbs, and legs.

References

1. R. O. Atienza and M. Ang, Jr. "A flexible control architecture for mobile robots: an application for a walking robot," *J. Intell. Robot. Syst.* **30**, 29–48 (2001).
2. C. M. Chew and G. A. Pratt, "Dynamic bipedal walking assisted by learning," *Robotica* **20**, 477–491 (2002).
3. S. Kajita, O. Matsumoto and M. Saigo, "Real-Time 3D Walking Pattern Generation for a Biped Robot With Telescopic Legs," *Proceedings of the IEEE International Conference on Robotics and Automation*, 3, 2299–2306, Seoul, Korea (May 21–26, 2001).
4. H. Hirukawa, S. Kajita, F. Kanehiro, K. Kaneko and T. Isozumi, "The human-size humanoid robot that can walk, lie down and get up," *Int. J. Robot. Res.* **24**(9), 755–769 (2005)
5. J. Nakanishi, J. Morimoto, G. Endo, G. Cheng, S. Schaal and M. Kawato, "Learning from demonstration and adaptation of biped locomotion," *Robot. Autonom. Syst.* **47**, 79–91 (2004).
6. M. M. Williamson, "Neural control of rhythmic arm movements," *Neural Netw.* **11**, 1379–1394 (1998).
7. M. S. Dutra, A. C. de P. Filho and V. F. Romano, "Modeling of a bipedal locomotor using coupled nonlinear oscillators of Van der Pol," *Biol. Cybern.* **88**(4), 286–292 (2004).
8. Y. Fukuoka, H. Kimura and A. H. Cohen, "Adaptive dynamic walking of a quadruped robot on irregular terrain based on

https://doi.org/10.1017/S026357470700344X Published online by Cambridge University Press

biological concepts," *Int. J. Robot. Res.* **22**(3–4), 187–202 (Mar.–Apr. 2003).
9. S. Miyakoshi, M. Yamakita and K. Furuta, "Juggling Control Using Neural Oscillators," *Proceedings of the IEEE/RSJ International Conference on Intelligent Robots and Systems* (1994) pp. 1186–1193.
10. S. Kotosaka and S. Schaal, "Synchronized Robot Drumming by Neural Oscillator," *Journal of the Robotics Society of Japan* **19**(1), 116–123 (2001).
11. A. Khoukhi, "Neural based RSPN multi-agent strategy for biped motion control," *Robotica* **19**, 611–617 (2001).
12. G. Taga, Y. Yamaguchi and H. Shimizu, "Self-organized control of bipedal locomotion by neural oscillators in unpredictable environment," *Biol. Cybern.* **65**, 147–159 (1991).
13. K. Matsuoka, "Sustaned oscillations generated by mutually inhibiting neurons with adaptation," *Biol. Cybern.* **52**, 367–376 (1985).
14. M. Vukobratovic, B. Borovac, D. Surla and D. Stokic, *Biped Locomotion—Dynamics, Stability, Control and Application* (Springer-Verlag, London, UK, 1990).
15. P. Sardain and G. Bessonnet, "Forces acting on a biped robot. Center of pressure—zero moment point," *IEEE Trans. Syst., Man, Cybern.—part A: systems and humans* **34**(5), 630–637 (2004).
16. A. Goswami, "Postural stability of biped robots and the foot-rotation indicator (FRI) point," *Int. J. Robot. Res.* **18**(6), 523–533 (1999).
17. H. K. Lum, M. Zribi and Y. C. Soh, "Planning and control of a biped robot," *Int. J. Eng. Sci.* **37**, 1319–1349 (1999).
18. C. Chevallereau and Y. Aoustin, "Optimal reference trajectories for walking and running of a biped robot," *Robotica* **19**, 557–569 (2001).
19. A. Takanishi, H. Lim, M. Tsuda and I. Kato, "Realization of Dynamic Biped Walking Stabilized by Trunk Motion on a Saggitally Uneven Surface," *Proceedings of the IEEE International Workshop on Intelligent Robots and Systems*, Ibaraki, Japan (1990) pp. 323–330.
20. Y. Ogura, *et al.*, "A Novel Method of Biped Walking Pattern Generation With Predetermined Knee Joint Motion," *Proceedings of the 2004 IEEE/RSJ International Conference on Intelligent Robots and Systems* 3, 2831–2836 (2004).
21. H.-O. Lim and A. Takanishi, "Compensatory motion control for a biped walking robot," *Robotica* **23**, 1–11 (2005).
22. Z. Michalewicz, "Genetic algorithms + data structures = evolution programs," *AI Series* (Springer-Verlag, New York, (1994).
23. "Biomechanics of motion," CISM Courses and Lectures **263**, 79–129 (1980).
24. J. Perry, MD, *Gait Analysis: Normal and Pathological Function* (McGraw Hill, New York, (1992) pp. 556.
25. C. L. Shih, "Gait synthesis for a biped robot," *Robotica* **15**, 599–607 (1997).
26. J. H. Park, "Fuzzy-logic zero-moment-point trajectory generation for reduced trunk motion of biped robots," *Fuzzy Sets Syst.* **134**, 189–203 (2003).
27. T. Arakawa and T. Fukuda, "Natural Motion Generation of Biped Locomotion Robot Using Hierarchical Trajectory Generation," *Proceedings of the 1997 IEEE International Conference on Robotics and Automations* (1997) pp. 211–216.
28. X. Mu and Q. Wu, "Synthesis of a complete sagittal gait cycle for a five-link biped robot," *Robotica* **21**, 581–587 (2003).
29. *Users Guide for Yobotics!* (Yobotics, Inc., Boston, MA, (2000–2003).
30. M. L. Lalash, *Control of Human Movement* (Human Kinetics Publishers, USA, (1994).
31. Y. Ogura, H. Aikawa, K. Shimomura, H. Kondo, A. Morishima, H. Lim and A. Takanish, "Development of a New Humanoid Robot to Realize Various Walking Pattern Using Waist Motions," *Springer CISM Courses and Lectures: Robotic Design, Dynamics, and Control* **487**, 279–286. Warsaw, Poland (2006).
32. T. Nagasaki, S. Kajita, K. Yokoi, K. Kaneko and K. Tanie, "Running Pattern Generation and Its Evaluation Using a Realistic Humanoid Model," *Proceedings of the 2003 IEEE International Conference on Robotics and Automation*, Taipet, Taiwan (2003) pp. 14–19.
33. A. N. Poo, M. H. Ang, Jr, C. L. Teo and Q. Li, "Performance of a neuro-model-based robot controller: adaptability and noise rejection," *Intell. Syst. Eng.* **1**(1), 50–62 (1992).

Appendix

Table A1. Parameters of GA, objective and penalty functions for flat-terrain walking Example 1 and 2.

Chromosome representation	Real-valued GA
Initial population M	150
Generation number T	250
Crossover[22]	Heuristic crossover
	Simple crossover
	Artistic crossover
Mutation[22]	Multi-nonuniform mutation
	Nonuniform mutation
	Uniform mutation
	Boundary mutation
Weights (objectives)	w_i = [15 50 10 40]
Weights (penalty)	p_i = [15 20 20 30 100 70]

Table A2. Parameters of GA, objective and penalty functions for 10° up-sloped terrain walking.

Chromosome representation	Real-valued GA
Initial population M	150
Generation number T	250
Crossover[22]	Heuristic crossover
	Simple crossover
	Arithmetic crossover
Mutation[22]	Multi-nonuniform mutation
	Nonuniform mutation
	Uniform mutation
	Boundary mutation
Weights (objectives)	w_i = [15 500 10 100]
Weights (penalty)	p_i = [10 50 20 30 500 80]

Table A3. Parameters of GA, objective and penalty functions for 10° down-sloped terrain walking.

Chromosome representation	Real-valued GA
Initial population M	150
Generation number T	250
Crossover[22]	Heuristic crossover
	Simple crossover
	Arithmetic crossover
Mutation[22]	Multi-nonuniform mutation
	Nonuniform mutation
	Uniform mutation
	Boundary mutation
Weights (objectives)	w_i = [12 500 10 100]
Weights (penalty)	p_i = [15 80 20 30 800 500]

https://doi.org/10.1017/S026357470700344X Published online by Cambridge University Press